Electronic Supplementary Material (ESI) for Materials Advances.

Supporting Information

Facile Surface Restructure by One-Step Sub-millisecond Laser Exposure Promotes the CO_2 Methanation Performance of Cobalt oxide supported Pd Nanoparticles with Copper-Oxide cluster decoration

Dinesh Bhalothia,[a†] Amisha Beniwal,[a†] Praveen Kumar Saravanan,[b] Guo-Heng Huang,[a] Mingxing Cheng,[a,c] Ming-Wei Lin,[a,d] Po-Chun Chen,[b*] Tsan-Yao Chen[a*]

Affiliations:

[a.] Department of Engineering and System Science, National Tsing Hua University, Hsinchu 30013, Taiwan
[b.] Department of Materials and Mineral Resources Engineering, National Taipei University of Technology, Taipei 10608, Taiwan
[c.] Department of Electrical Engineering and Electronics, University of Liverpool, Liverpool L69 3GJ, UK
[d.] Institute of Nuclear Engineering and Science, National Tsing Hua University, Hsinchu 30013, Taiwan

[†] denotes equal contribution of authors.

Corresponding Author:

Tsan-Yao Chen
Email: chencaeser@gmail.com
Tel: +886-3-5715131 # 34271
FAX: +886-3-5720724

Po-Chun Chen
Email: cpc@mail.ntut.edu.tw
Tel: +886-2-27712171 # 2729
FAX: +886-2-27317185

1. Gaseous Product Analysis

To calibrate the system, standard gases including H_2 and CO (each at a concentration of 200 ppm), as well as CH_4, C_2H_6, and C_3H_8 (each at a concentration of 100 ppm) balanced in "He," were procured from ECGAS Asia (Taiwan). Different concentrations of these gases were prepared by introducing them into sampling loops of varying sizes. The gas cylinder was directly connected to a 6-port switching valve to fill the sampling loop, which was subsequently injected into the GC column for analysis. Gas samples were collected directly from the thermal catalytic reactor to evaluate performance. The experiment was conducted using an automatic premixed gas supply apparatus equipped with a heating block, wherein the selected catalyst was packed into a glass tube to form a thermal reaction bed. The glass tube had dimensions of 100 mm in length, 1 mm in thickness, and a 2 mm inside diameter. The temperature of the reaction bed was controlled by a thermal controller with a PID algorithm, allowing users to set up an analytical method with desired reaction time, temperature, and flow rate. Additionally, self-designed software served as the interface to remotely initiate a GC analysis. The total flow rate of the gases was measured and regulated by a mass flow controller (MFC). All gaseous samples from the reaction bed were analyzed using a gas chromatograph (GC) instrument (Agilent 7890, USA) equipped with a Valco PDHID detector (model D-3-I-7890, VICI, USA) and a micro-packed column-filled with carbon molecular sieve (Shincarbon ST, 2 m x 1.0 mm i.d.; Restek Chromatography Products, USA). The gas samples were introduced into the GC column through a 6-port switching valve (A6C6UWT, VICI) from the sampling loop, injecting a fixed volume of sample (160 μL). Ultra-high-purity helium (UHP) (99.9995%) was used as both the carrier gas and discharge gas, with two heated helium purifiers (HP2 and HPM, VICI, USA) positioned between the cylinder and the flow splitter to remove impurities from the UHP helium and stabilize the baseline. The helium flow rate was set at 30 ml/min using a restrictor (30 cc/min 60 psi He, VICI). The carrier gas operated in constant pressure mode at 90 psi, controlled by a pressure control module (PCM, Agilent). The oven temperature was programmed from 308 K (1.5 min) to 553 K (ramping at 20 K/min), holding for 3.25 min. Stainless steel tubing was employed throughout the thermal

reactor and the GC's sampling system, with all connectors being tested for leaks using an electric leak detector. The catalytic reaction bed was enclosed in a heating block operating at near-atmospheric pressure. A mixture of 12 mg of the catalyst and 23 mg of silica gel (60/80 mesh, Alltech, USA) was placed inside a glass tube (2 mm ID × 3 mm OD, 100 mm length), with quartz wool plugs at both ends. In the initial step, N_2 gas (50 mL/min) was introduced into the reactor bed at room temperature (RT) for one hour to remove moisture from the catalyst. Subsequently, a gas stream of either pure CO_2 or a CO_2-H_2 mixture (CO_2:H_2 = 1 : 3) was introduced at a flow rate of 20 mL/min into the reaction bed, within a temperature range of 323 to 573 K. After maintaining the isothermal temperature for 30 minutes, gas products were injected into the analytical column from the sampling loop for GC analysis. The detection system's sensitivity was approximately 0.1 ppm.

2. HRTEM images control samples.

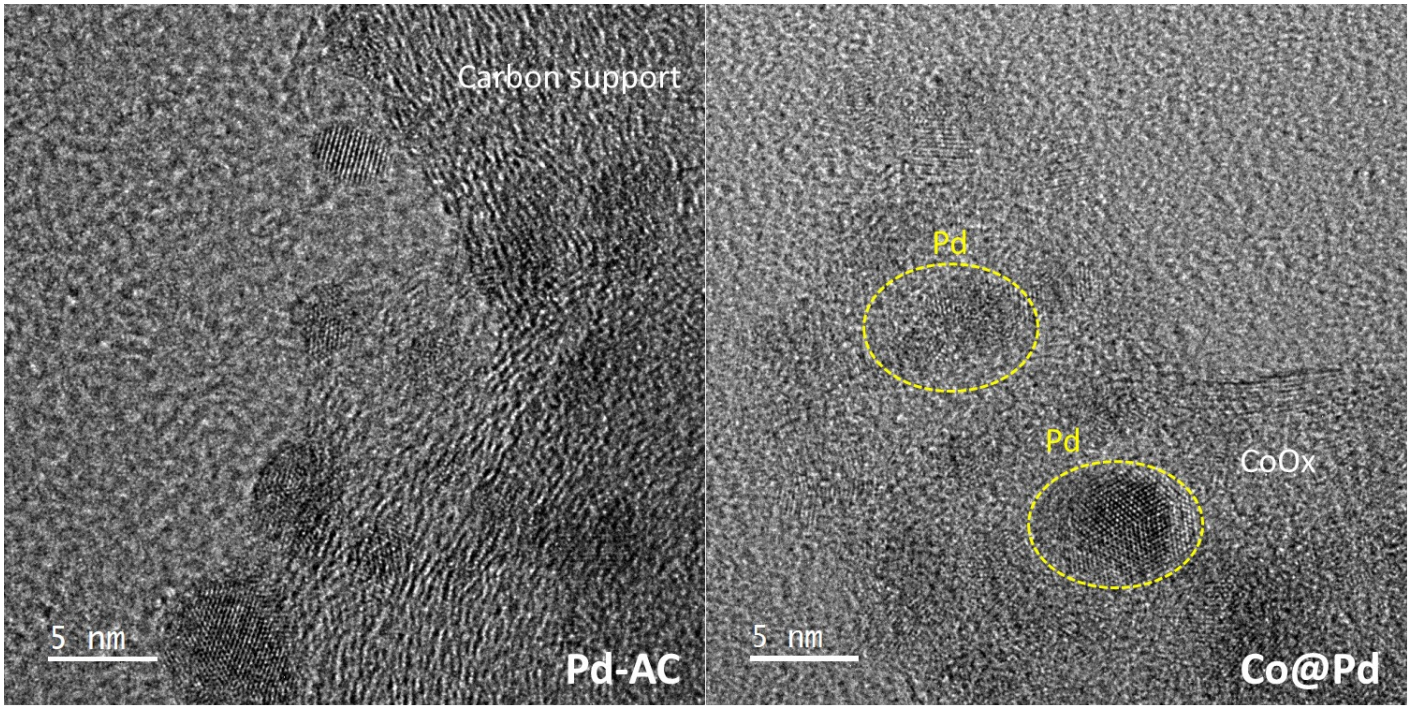

Figure S1. HRTEM images of as-prepared (a) Pd-AC and (b) Co@Pd.

3. HRTEM images control samples.

Figure S2 shows the XRD patterns of CPCu NCs and reference samples (Co, Pd and Co@Pd), where the four characteristic peaks M, N, O and P, respectively, correspond to the diffraction lines from the (111), (200), (220) and (311) planes of the metallic Pd crystal. Meanwhile, peak X refers to the (002) facet of the carbon support, while peaks P and Q correspond to the Co_3O_4 (311) and Co_2Pd (1 0 -1 3) planes, respectively. Notably, the Co NPs exhibit the suppressed and broadened peak profile, suggesting the formation of amorphous and/or short-range disordered Co-oxide. Furthermore, Co@Pd exhibits significantly broadened diffraction signals along with higher background (h) as compared to Pd nanoparticles. These results are consistent with the HRTEM observation (**Figure S1b**), where high surface roughness and a certain extent of surface defects are observed in the Pd domains. Meanwhile, the offset of diffraction peaks to the lower angles indicates the increased lattice spacing, which can be attributed to the severe lattice mismatch between the Co and Pd domains at the binary interface and the formation of subnanometer scale CoPd alloy structures. These scenarios are further confirmed by the presence of peak Q, which corresponds to the Co_2Pd (1 0 -1 3) planes. Furthermore, the suppressed peak intensity suggests the disruption of atomic arrangement in the Pd domains due to the decorated Cu species and their subsequent oxidation on the surface of pristine CPCu NC. On the other hand, the highest peak intensity of CPCu-1 NC confirms the removal of the surface oxide layer due to laser exposure. Further raising the per pulse energy to 10 mJ leads to a higher extent of atomic migration, therefore, the Co atoms from the core region are expected to migrate on the surface. In this case, the presence of both CuOx and CoOx is obvious on the surface of CPCu-10 NC, hence, the long-range order is suppressed and diffraction signals are suppressed as compared to CPCu-1 NC.

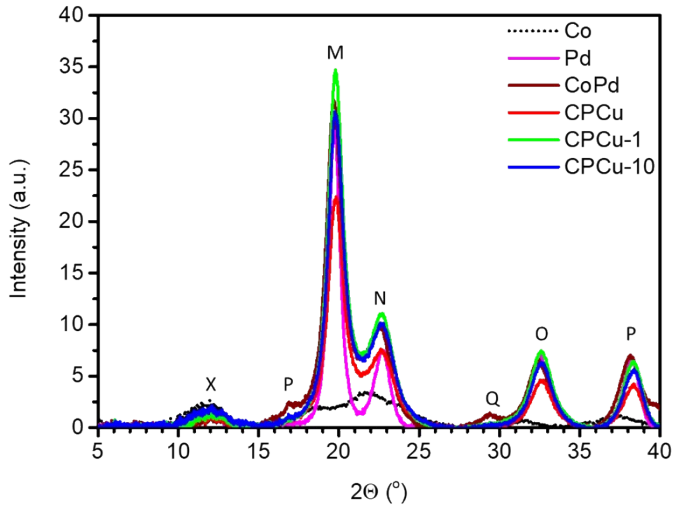

Figure S2. The comparative XRD patterns of experimental CPCu NCs and reference samples (Co, Pd and Co@Pd) The wavelength of incident X-ray for XRD measurement is 0.6888 Å (18.0 KeV).

4. Model analysis fitting curves compared with experimental FT-EXAFS spectra at Cu K-edge.

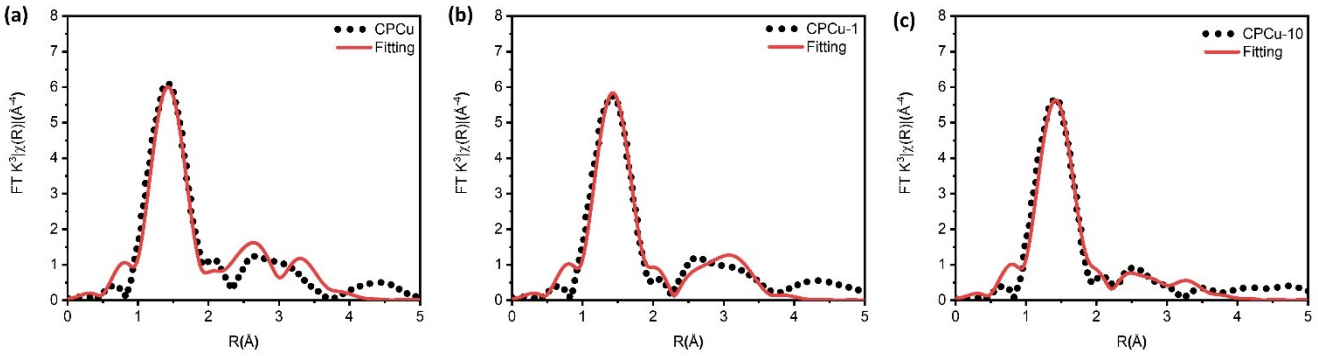

Figure S3. Model analysis fitting curves compared with experimental FT-EXAFS spectra at Cu K-edge of (a) CPCu, (b) CPCu-1 and (c) CPCu-10 samples.

5. Model analysis fitting curves compared with experimental FT-EXAFS spectra at Pd K-edge.

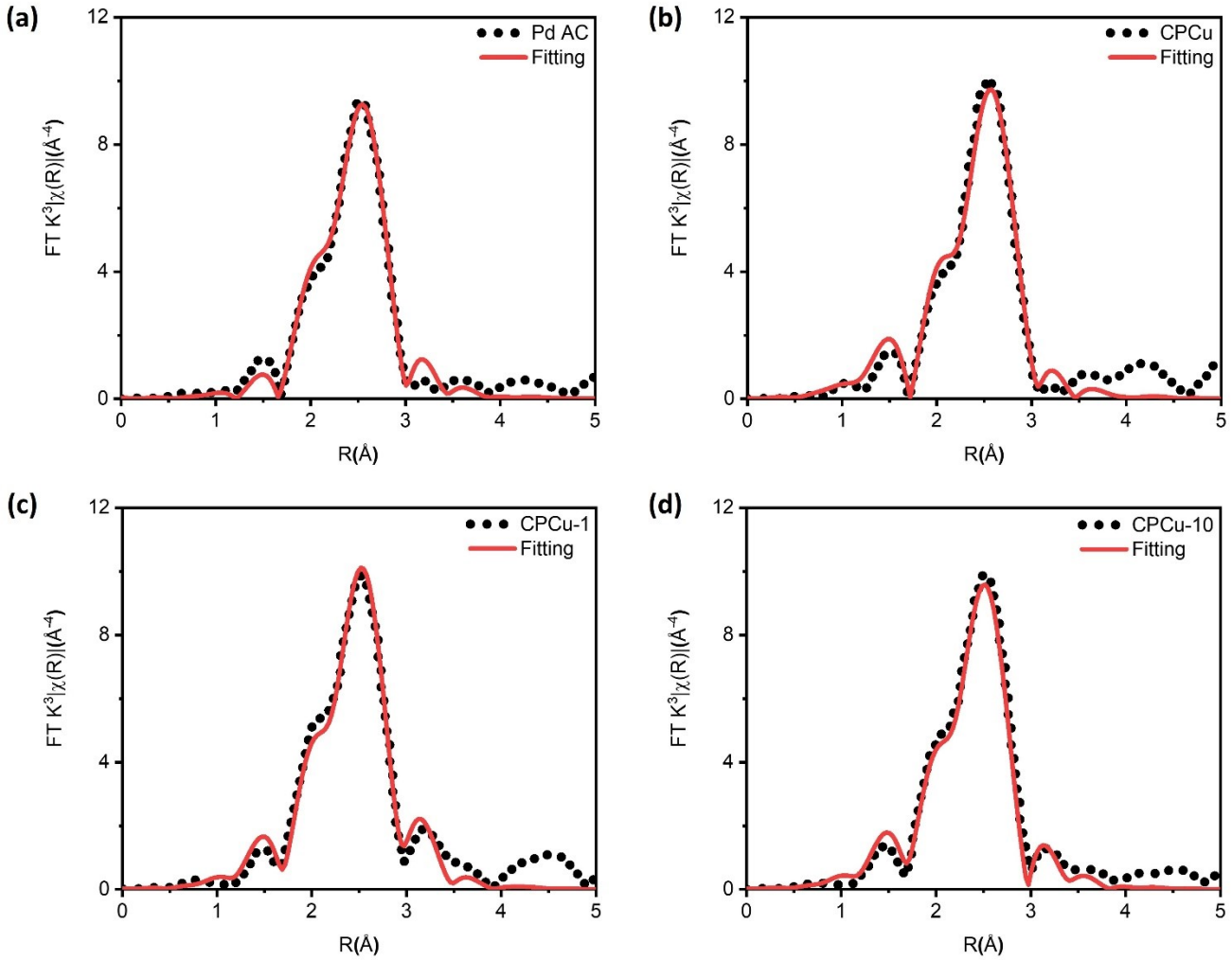

Figure S4. Model analysis fitting curves compared with experimental FT-EXAFS spectra at Pd K-edge of (a) Pd-AC, (b) CPCu, (c) CPCu-1 and (d) CPCu-10 samples.

6. Model analysis fitting curves compared with experimental FT-EXAFS spectra at Co K-edge.

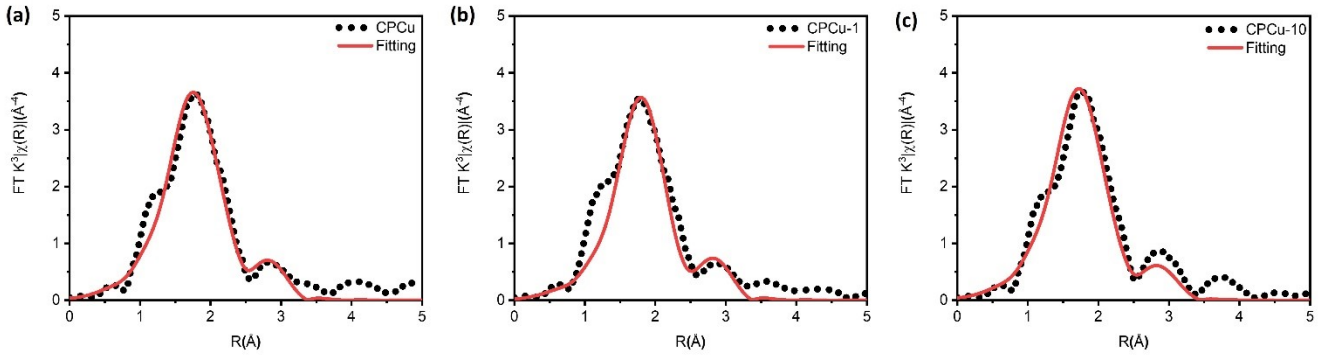

Figure S5. Model analysis fitting curves compared with experimental FT-EXAFS spectra at Co K-edge of (a) CPCu, (b) CPCu-1 and (c) CPCu-10 samples.

7. Comparative XPS spectra of Co@Pd compared with bare Pd nanoparticles at Pd-3d orbitals.

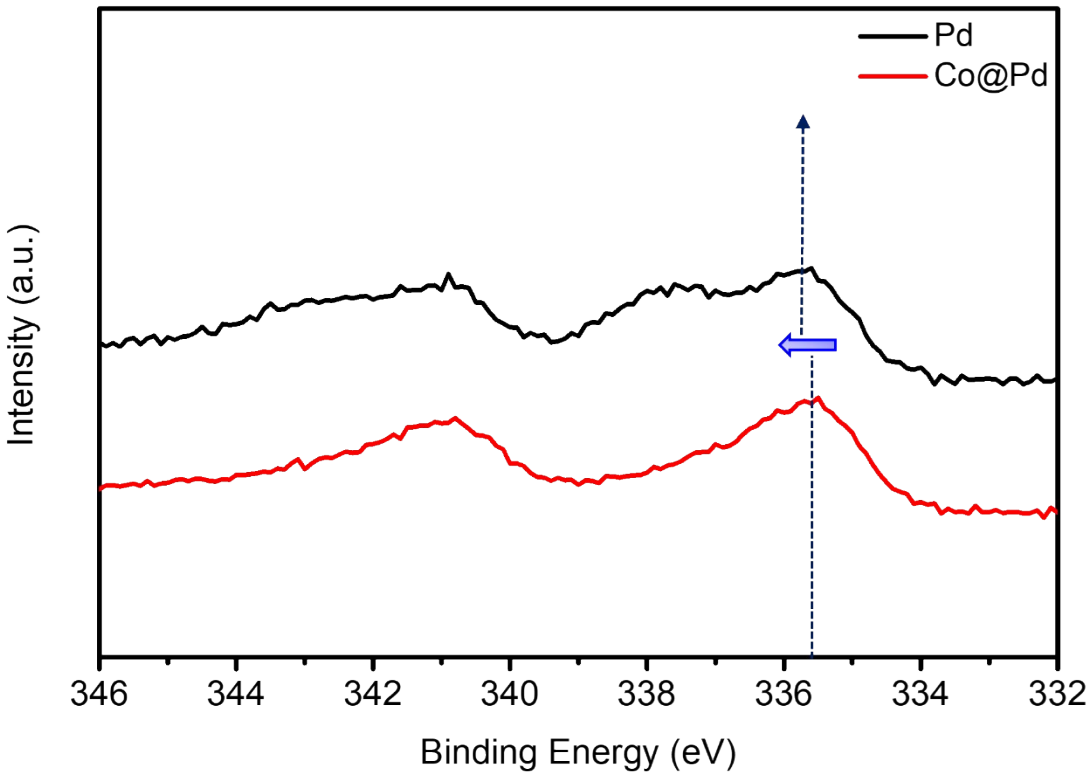

Figure S6. Comparative XPS spectra of Co@Pd compared with bare Pd nanoparticles at Pd-3d orbitals.

8. Calculated activation energy of CO and CH4 production in the presence of reaction gases (CO2+3H2).

Table S1. Calculated activation energy of CO and CH_4 production in the presence of reaction gases (CO_2+3H_2).

CO_2 + H_2	CO activation energy (eV)			CH_4 activation energy (eV)		
Temperature (°C)	CPCu	CPCu-1	CPCu-10	CPCu	CPCu-1	CPCu-10
(50 – 100)		N/A		0.10	0.08	0.06
(100 - 150)				0.61	1.26	0.98
(150 - 200)	1.39		1.27	1.86	1.60	1.93
(200 - 250)	0.78	0.85	0.51	1.25	1.05	0.64
(250 - 300)	0.22	0.16	0.17	0.16	0.16	0.14

9. Gas Chromatography (GC) determined CO_2RR results for the CPCu NCs and reference samples.

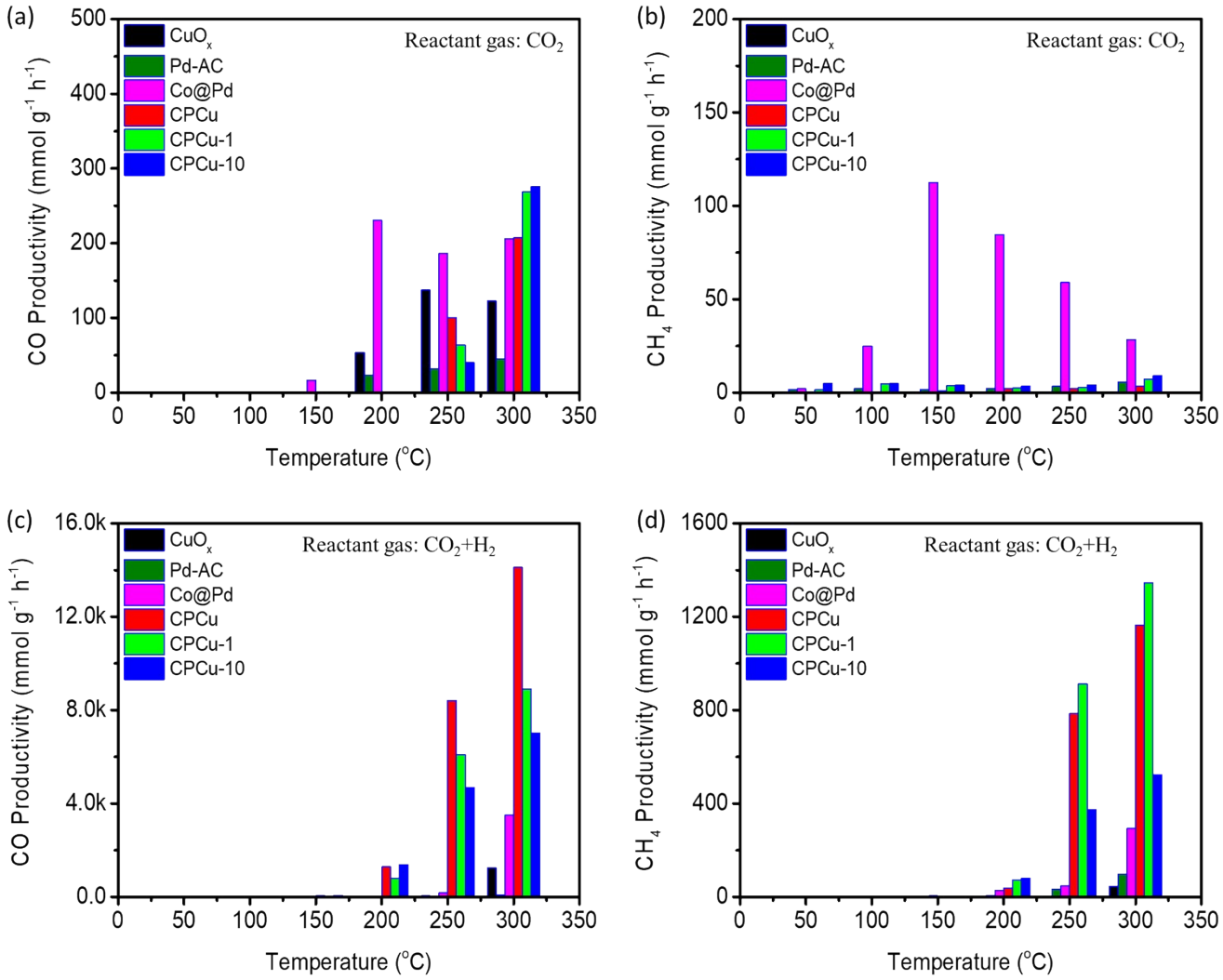

Figure S7. Gas Chromatography (GC) determined CO_2RR results for the CPCu NCs and reference samples for (a) CO and (b) CH_4 productivity in pure CO_2 ambient. Results for CO and CH_4 productivity in reaction gas (CO_2+3H_2) are respectively demonstrated in (c) and (d).

10. Benchmark for the CO_2RR performances of heterogeneous NCs.

Table S2. Benchmark table for the CO_2RR performance of heterogeneous NCs.

Sample	Temp. (K)	Reaction gas	Production$_{CH4}$			References
			ppm	(μmol g^{-1})	(mmol g^{-1} h^{-1})	
CPCu-1	300°C	CO_2: H_2 = 1: 3	109.95	373.83	1345.78	This Study
0.1% Pd, 10%Ni, 6.1% "Na_2O"	500°C	7.5% CO_2, 15% H_2/N_2		180.0		1
0.1% Pt, 10%Ni, 6.1% "Na_2O"	500°C			160.0		
1% Pt, 10%Ni, 6.1% "Na_2O"	500°C			250.0		
1% Ru, 10% Ni, 6.1% "Na_2O"	320°C			380.0		
Ru15%CaO	400°C	1.4% CO_2+ 10% H_2		414		2
Ru10%Na_2CO_3	310°C			383		
CNP	300°C	CO_2: H_2 = 1: 3	49.81	169.35		3
CNP-1			59.29	201.58		
CNP-10			51.59	175.40		

*The CH_4 prodcution yield has been changed from ppm to umol g^{-1} (ppm * 3.4 = umol g^{-1}) and umol g^{-1} to mmol g^{-1} h^{-1} (umol g^{-1} *3600/1000 = mmol $g^{-1}h^{-1}$)

Reference

1. M. A. Arellano-Treviño, N. Kanani, C. W. Jeong-Potter and R. J. Farrauto, *Chemical Engineering Journal*, 2019, **375**, 121953.

2. A. Bermejo-López, B. Pereda-Ayo, J. A. González-Marcos and J. R. González-Velasco, *Applied Catalysis B: Environmental*, 2019, **256**, 117845.

3. D. Bhalothia, W.-H. Hsiung, S.-S. Yang, C. Yan, P.-C. Chen, T.-H. Lin, S.-C. Wu, P.-C. Chen, K.-W. Wang, M.-W. Lin and T.-Y. Chen, *ACS Applied Energy Materials*, 2021, **4**, 14043-14058.